



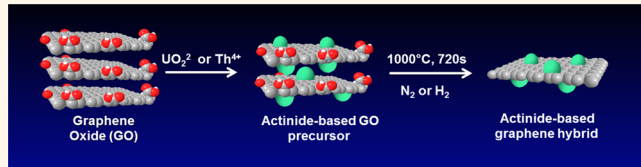
Uranium- and Thorium-Doped Graphene for Efficient Oxygen and Hydrogen Peroxide Reduction

Zdeněk Sofer,^{†,*} Ondřej Jankovský,[†] Petr Šimek,[†] Kateřina Klímová,[†] Anna Macková,^{‡,§} and Martin Pumera^{||,*}

[†]Department of Inorganic Chemistry, Institute of Chemical Technology, Technická 5, 166 28 Prague 6, Czech Republic, [‡]Nuclear Physics Institute of the ASCR, v.v.i., 250 68 Řež, Czech Republic, [§]Department of Physics, Faculty of Science, J.E. Purkyně University, 400 96 Ústí nad Labem, Czech Republic, and ^{||}Division of Chemistry & Biological Chemistry, School of Physical and Mathematical Sciences, Nanyang Technological University, 637371 Singapore

ABSTRACT Oxygen reduction and hydrogen peroxide reduction are technologically important reactions in the fields of energy generation and sensing. Metal-doped graphenes, where metal serves as the catalytic center and graphene as the high area conductor, have been used as electrocatalysts for such applications.

In this paper, we investigated the use of uranium-graphene and thorium-graphene hybrids prepared by a simple and scalable method. The hybrids were synthesized by the thermal exfoliation of either uranium- or thorium-doped graphene oxide in various atmospheres. The synthesized graphene hybrids were characterized by high-resolution XPS, SEM, SEM-EDS, combustible elemental analysis, and Raman spectroscopy. The influence of dopant and exfoliation atmosphere on electrocatalytic activity was determined by electrochemical measurements. Both hybrids exhibited excellent electrocatalytic properties toward oxygen and hydrogen peroxide reduction, suggesting that actinide-based graphene hybrids have enormous potential for use in energy conversion and sensing devices.



KEYWORDS: graphene · actinides · electrochemistry · oxygen reduction · uranium

At present, there is a great demand for electrocatalytic devices for energy systems and sensors. In particular, there is a need to find new oxygen reduction reactions (ORR) for fuel cells and oxygen–Zn batteries that replace the traditional Pt/C systems.¹ Graphene-based hybrids seem to be a promising candidate for such purposes.

Graphene, a sp^2 -bonded carbon network in a honeycomb lattice,² has been intensively studied due to its interesting electrical, optical, and mechanical properties, as well as its high surface area. Graphene can be used in photovoltaics,³ catalysis,⁴ electrochemical sensing,⁵ and for energy production and storage.⁶ Various chemical modifications can be applied to significantly enhance its properties.^{7–9} The properties of graphene can also be modified by doping it with various additives. Doping with even a small amount of metal nanoparticles leads to the formation of graphene hybrids that can be suitable for electrocatalysis.

Various methods of synthesizing doped graphene hybrids have been reported.^{10–13}

The electrocatalytic effects of such doping usually lead to a shift in potential of tens of millivolts. In such hybrids, a graphene sheet acts as the current collector and supports the catalyst. Theoretical aspects of ORR processes for Pt-, Fe-, and Al-doped graphene have been intensively studied in recent years.^{14,15}

Although such a catalyst is typically a transition metal, we wondered if an actinide-based catalyst might be even more effective. For example, uranium has proved itself useful in catalysis in recent years.^{16,17} Although uranium, like thorium, is a radioactive element, they have sufficiently long half-lives to be safely used on a large scale: the half-lives of their two most stable isotopes (^{238}U and ^{232}Th) are \sim 4.5 billion years and \sim 14 billion years, respectively.¹⁸

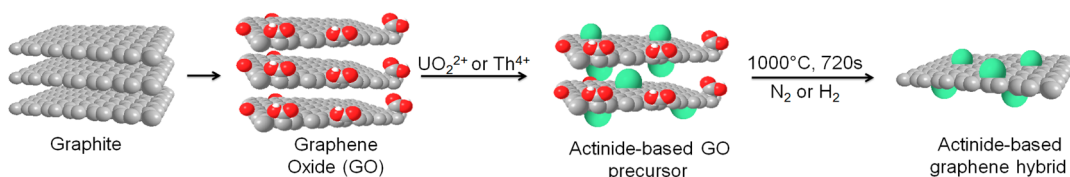
Despite this, thus far, nothing has been published in the literature about the use of uranium- or thorium-doped graphenes in electrocatalysis. In this paper, we show that actinide-based graphene hybrids can be used for highly efficient oxygen and

* Address correspondence to pumera@ntu.edu.sg, zdenek.sofcer@vscht.cz.

Received for review April 11, 2014 and accepted June 30, 2014.

Published online June 30, 2014
10.1021/nn502026k

© 2014 American Chemical Society



Scheme 1. Synthesis of actinide-based graphene hybrids.

hydrogen peroxide reduction reactions. Both hybrids were prepared by the thermal exfoliation and reduction of doped graphene oxides in hydrogen and nitrogen atmospheres. We describe the effects of the different atmospheres and the influence of the dopant on the hybrids' electrocatalytic activity.

RESULTS AND DISCUSSION

We created U-doped and Th-doped graphene oxides (Hofmann method) by exposing graphene oxide to either uranium or thorium salt. The doped graphene oxide slurries (labeled U-GO and Th-GO) were subsequently thermally exfoliated and reduced in a hydrogen or nitrogen atmosphere. The synthesis of these actinide-based graphene hybrids is shown in Scheme 1. The formed graphene hybrids (labeled according to actinide type and exfoliation atmosphere as U-H, U-N, Th-H, and Th-N) were then characterized using various methods and their electrocatalytic properties determined.

First, the morphology of the U-GO and Th-GO precursors was analyzed by scanning electron microscopy (SEM) and SEM/energy-dispersive X-ray spectroscopy (SEM-EDS). The SEM images show that both samples have the platelet structure typically observed for graphene oxide samples (Supporting Information Figure SI1). It is not possible to recognize the actinide dopants in either sample, which indicates that the size of the doping particles was in the range of nanometers or sub-nanometers.

The distribution and concentration of individual elements within the precursors were measured by SEM-EDS. The distribution of the major elements (C, O, and U/Th) is shown in Figure SI2, from which it can be observed that U and Th were distributed homogeneously in both precursors. In U-GO, the concentrations were 76.6 wt % of C, 21.6 wt % of O, and 1.4 wt % of U; for Th-GO, the concentrations were 83.4 wt % of C, 15.2 wt % of O, and 0.7 wt % of Th. In both samples, low concentrations of S and Cl were found as impurities. It is likely that the Th and U were bonded to the graphene oxide surface by carboxyl and hydroxyl groups. The highly uniform distribution of all elements is documented by the SEM-EDS concentration maps.

After thermal reduction and exfoliation, the hybrids were also analyzed by SEM. Whether exfoliated in nitrogen or hydrogen, every hybrid exhibited similar lamellar "worm-like" structures, thereby confirming the successful formation of thermally reduced graphene

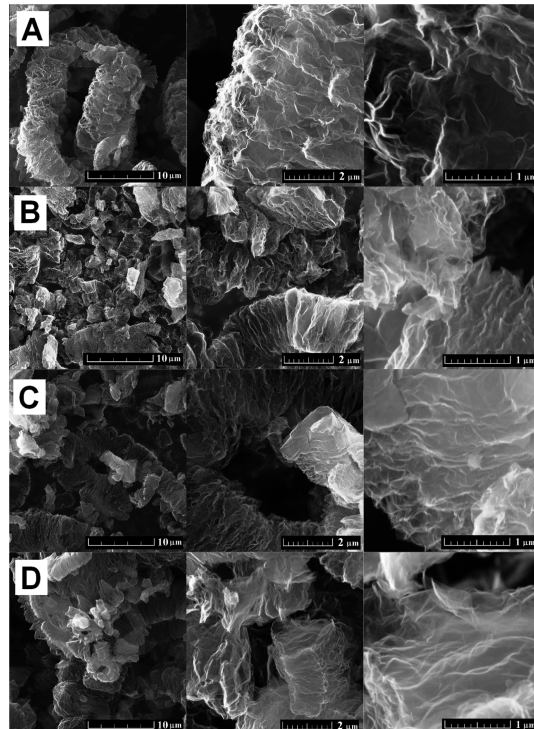


Figure 1. Morphology of actinide-based graphene hybrids obtained by SEM: (A) U-H, (B) U-N, (C) Th-H, (D) Th-N.

(Figure 1). However, it was not possible to identify and visualize the individual actinide dopants on the graphene sheets.

SEM-EDS showed that the distribution of O, Th, and U was highly uniform in all hybrids (Figure 2). In U-H, the concentrations were 91.3 wt % of C, 6.4 wt % of O, and 1.5 wt % of U; in U-N, the concentrations were 89.1 wt % of C, 8.4 wt % of O, and 1.3 wt % of U. These results show that U-H was more reduced than U-N. In Th-H, the concentrations were 96.2 wt % of C, 3.0 wt % of O, and 0.5 wt % of Th; in Th-N, the concentrations were 96.3 wt % of C, 3.2 wt % of O, and 0.4 wt % of Th. Thus, the oxygen concentration was lower in the graphene hybrids exfoliated in a hydrogen atmosphere. All of the graphene hybrids contained small amounts of S and Cl originating from the graphene oxide precursors.

Scanning transmission electron microscopy (STEM) was used, at various magnifications, to investigate the structures of the hybrids. The graphenes exhibited a typical wrinkled structure, but no actinide particles were observed (Figure 3). Together with the SEM-EDS maps, this further illustrates the highly uniform

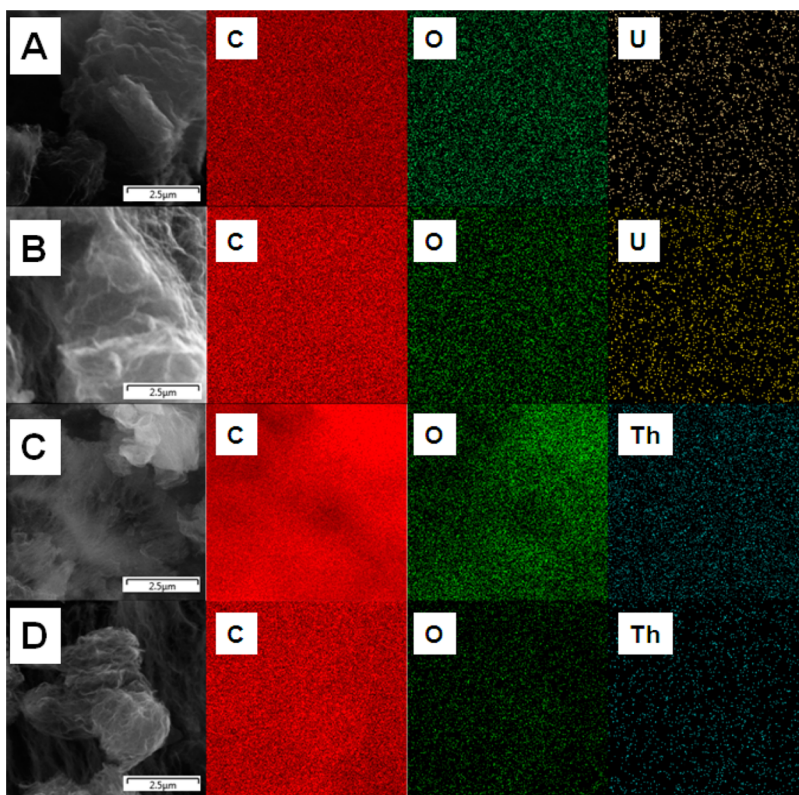


Figure 2. Elemental distribution maps of actinide-based graphene hybrids obtained by SEM-EDS: (A) U-H, (B) U-N, (C) Th-H, (D) Th-N.

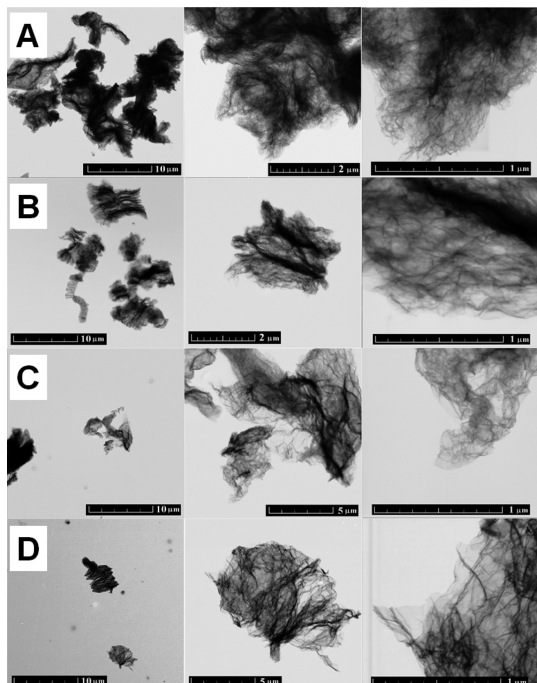


Figure 3. STEM images of actinide-based graphene hybrids: (A) U-H, (B) U-N, (C) Th-H, (D) Th-N.

distribution of the actinide particles, which did not appear to agglomerate.

To determine the overall composition of the graphene precursors, the composition of all samples was

compared to the results obtained from combustible elemental analysis (CHNS-O). The U-GO sample was composed of 54.28 wt % C, 1.91 wt % H, and 43.82 wt % O; the Th-GO was composed of 55.77 wt % C, 1.96 wt % H, and 42.27 wt % O.

After exfoliation/thermal reduction, the composition obviously changed. In terms of the U-doped graphenes, U-H was composed of 92.15 wt % C, 0.63 wt % H, 0.05 wt % N, and 7.18 wt % O, while U-N was composed of 81.97 wt % C, 1.18 wt % H, 0.47 wt % N, and 7.18 wt % O. In terms of the Th-doped graphenes, Th-H was composed of 96.80 wt % C, 0.51 wt % H, 0.05 wt % N, and 2.66 wt % O, while Th-N was composed of 96.35 wt % C, 0.34 wt % H, 0.04 wt % N, and 3.28 wt % of O. The data were recalculated to atom % as shown in Supporting Information (Table S1).

The oxygen concentration was always lower for the samples exfoliated in a hydrogen atmosphere, which is to be expected with exfoliation in a reducing atmosphere. Interestingly, the concentration of H was higher than O in atom %. This can be explained by the formation of C–H bonds during the thermal exfoliation of the doped graphene oxides. In the oxygen functional groups, the H/O ratio is 1 in a hydroxyl group, 0.5 in carboxylic acid, and 0 for ketone and epoxide. Therefore, if we assume that oxygen is present only in the form of hydroxyl groups, the minimum concentration of C–H can be calculated. Our calculations showed that the minimum theoretical concentrations

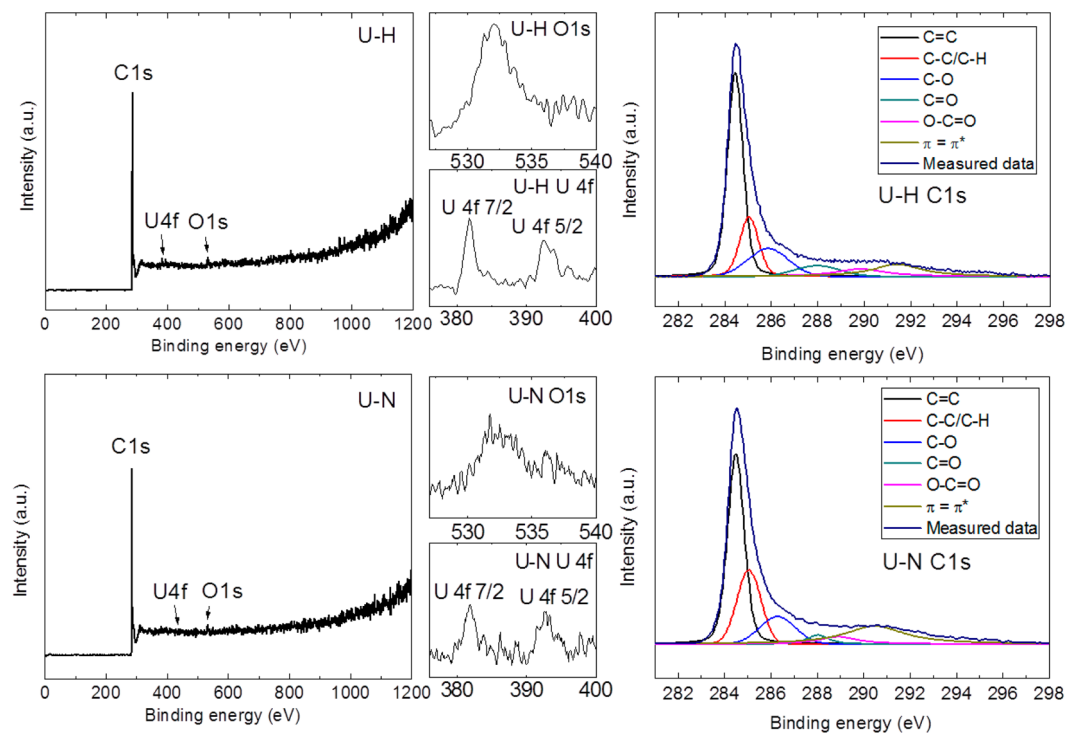


Figure 4. XPS spectra of uranium–graphene hybrids; survey spectra U-H and U-N on the left, U 4f details in the middle, and high-resolution XPS spectra of C 1s signal on the right.

of C–H were 1.6 atom % for Th-N, 2.1 atom % for U-N, 2.2 atom % for U-H, and 4.2 atom % Th-H. Of course, the actual concentrations were even higher, possibly much higher. The graphenes exfoliated in nitrogen had lower concentrations of hydrogen compared to those exfoliated in hydrogen. Although actinide ions can act as hydrogenation catalysts for the introduction of hydrogen into a graphene framework, the explanation for such a mechanism is not obvious.

High-resolution X-ray photoelectron spectroscopy (XPS) was used to analyze chemical composition and structure. The XPS spectra of the U-graphene hybrids are shown in Figure 4. Peaks were detected at 284.5 eV for C 1s, 532.5 eV for O 1s, 381.8 eV for U 4f_{7/2}, and 392.8 eV for U 4f_{5/2}; however, the O 1s and U 4f peaks were of very low intensity. The energies of the U 4f peaks indicated the presence of uranium, either in the form of UO₃ or in a mixed-valence state such as U₃O₈. It is also possible that some part of the uranium was in the form of carbide.¹⁹

The detailed high-resolution XPS spectra of C 1s showed a single peak at 284.5 eV with an asymmetrical tail at higher energies (Figure 4). Careful curve fitting was performed on both C 1s spectra to quantitatively differentiate the different carbon stages: C=C (284.5 eV); C–C/C–H (285.1 eV); C–O of alcohol/ether groups (286.2 eV); the C=O of carbonyl groups (287.4 eV); O–C=O of carboxylic acid/ester groups (289.1 eV); and the π – π^* interaction (291.0 eV). The relative abundance of these functional groups is shown in Table 1. The high concentration of the C–C band, which has a

TABLE 1. Quantitative Comparison of Individual Carbon Stages in C 1s Obtained by High-Resolution XPS

groups	concentration (%)			
	U-H	U-N	Th-H	Th-N
C=C	53.4	41.0	50.2	55.4
C–C/C–H	18.7	20.6	18.9	16.8
C–O	17.1	11.4	8.1	7.9
C=O	7.4	3.1	8.1	7.7
O–C=O	8.5	5.1	5.9	1.0
π – π^*	13.5	18.8	8.9	11.2

similar energy to C–H, may also indirectly indicate the presence of the above-mentioned C–H bond.

XPS analysis was also performed for the Th-graphene hybrids. Peaks were detected at 284.5 eV for C 1s, 532.5 eV for O 1s, 334.2 eV for Th 4f_{7/2}, and 343.5 eV for Th 4f_{5/2} (Figure 5). The energies of the Th 4f peaks indicated the presence of thorium in the form of ThO₂. It is also possible that some part of the thorium was in the form of carbide because carbide can be formed on the Th-graphene interface at elevated temperatures.²⁰ C 1s curve fitting showed the relative abundance of the individual functional groups (Table 1). Compared to the U-doped hybrids, the Th-doped hybrids had slightly higher concentrations of the C–C/C–H bond. This indicates a higher concentration of C–H functional groups, which was also confirmed by the elemental analysis.

The C/O ratios (atom %) were calculated from the XPS survey spectra for all four actinide-based graphene

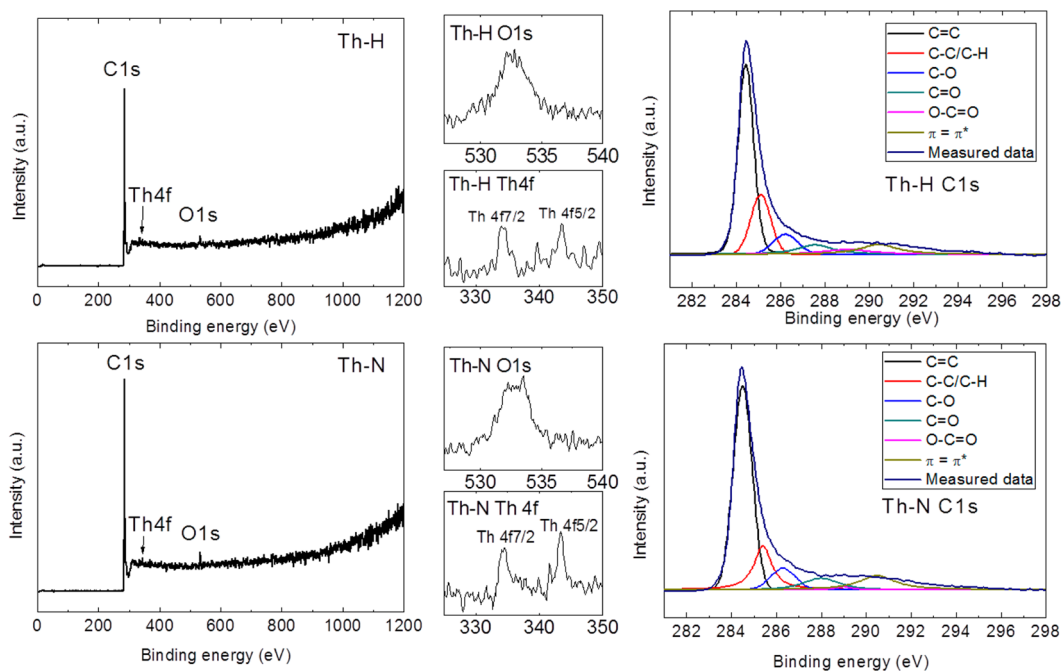


Figure 5. XPS spectra of thorium–graphene hybrids; survey spectra Th-H and Th-N on the left, Th 4f details in the middle, and high-resolution XPS spectra of C 1s signal on the right.

TABLE 2. Comparison of C/O Ratios Obtained by SEM/Energy-Dispersive X-ray Spectroscopy, Combustible Elemental Analysis, and High-Resolution X-ray Photoelectron Spectroscopy

	atom % C/O		
	SEM-EDS	CHNS-O	XPS
U-N	14.12	6.66	60.3
U-H	19.05	17.05	58.5
Th-N	40.10	39.17	49.0
Th-H	42.76	48.49	53.9

hybrids and compared with the results obtained from the other analytical techniques (Table 2). The results were in relatively good agreement, thus confirming the synthesis of highly reduced actinide-based graphene hybrids.

To determine the quality of the supporting graphene layer, we used Raman spectroscopy. The Raman spectra showed two major bands (Figure 6). The first band, the D band associated with sp^3 defects in the sp^2 lattice, gives a signal at $\sim 1350\text{ cm}^{-1}$. The second band, the G band associated with a pristine sp^2 graphene lattice, gives a signal at $\sim 1560\text{ cm}^{-1}$.²¹ The ratio between the D and G band intensities (D/G ratio) indicates the degree of disorder in a carbon structure. In our case, higher values were observed for the graphene hybrids exfoliated in a hydrogen atmosphere. This effect may be due to a number of factors but is most likely caused by the hydrogenation of the graphene skeleton catalyzed by the presence of actinide ions combined with the enhanced effect of graphene etching in a hydrogen atmosphere.

The Raman spectroscopy results were also used to determine the average crystallite size (L_a) by applying the following equation:²²

$$L_a = 2.4 \times 10^{-10} \times \lambda_{\text{laser}}^4 \times I_G/I_D \quad (\text{eq 1})$$

where I_G/I_D is the ratio of the intensities of the D and G bands and λ_{laser} refers to the laser wavelength. The D/G ratios and corresponding crystallite sizes of the four hybrids are summarized in Table 3.

The inherent electrochemistry of the hybrids was investigated in 50 mM phosphate buffer. A GC electrode and undoped thermally reduced graphene (TRG) were used as controls. While the controls showed no peak, the cyclic voltammograms for the hybrids showed an intense peak with its maximum around 0.15–0.20 V (Figure 7). This peak likely originated from the oxidation of the doping atoms.

The heterogeneous electron transfer (HET) rates of the hybrids were evaluated using a $[\text{Fe}(\text{CN})_6]^{3-/-4-}$ redox probe in 50 mM PBS as a supporting electrolyte (Figure 8). The HET rates were calculated using Nicholson's equation.²³ The peak-to-peak separation values and the HET rate constants are shown for all samples and controls (Table 4). The peak-to-peak separation was almost identical for both of the U-doped graphenes: 0.168 V for U-N and 0.172 V for U-H. A greater difference was observed between the Th-doped samples: 0.181 V for Th-N and 0.146 V for Th-H. Compared with these results, the GC electrode and TRG sample exhibited significantly slower HET rates, as shown by peak-to-peak separation values of 0.324 and 0.241 V, respectively. These results show that doping graphene with actinides significantly improves HET rates.

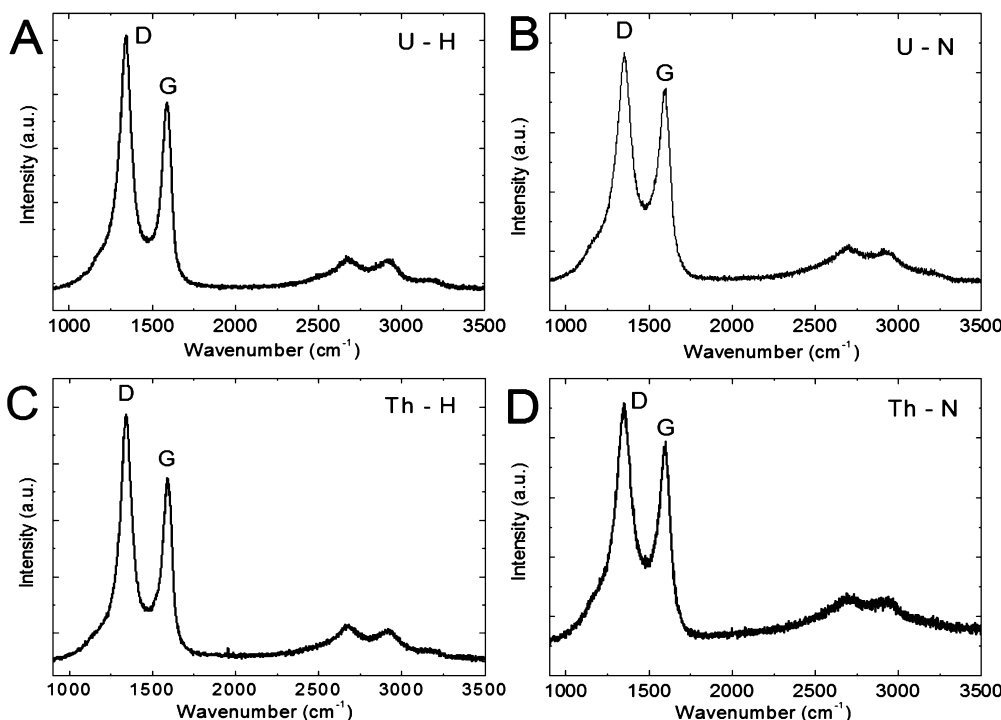


Figure 6. Raman spectra of actinide-doped graphene hybrids.

TABLE 3. D/G Ratios and Corresponding Crystallite Sizes Measured by Raman Spectroscopy

sample	D/G	L_a (nm)
Th-H	1.29	14.9
Th-N	1.16	16.5
U-H	1.32	14.6
U-N	1.15	16.7

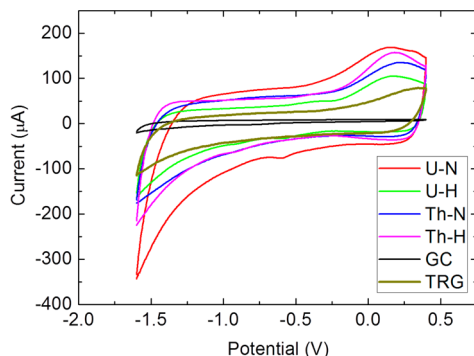


Figure 7. Inherent electrochemistry of U- and Th-doped graphene hybrids. Conditions: 50 mM PBS, pH 7.0, scan rate 100 mV/s.

The oxygen reduction reaction is of major importance in energy conversion and storage devices, such as fuel cells and zinc–air batteries.²⁴ However, there is an urgent need for the development of efficient low-cost catalysts in both acidic and basic media.^{25–35} Electrochemical measurements of the oxygen reduction reaction showed that oxygen reduction in an alkaline environment had a dramatic electrocatalytic effect. Oxygen reduction for Th-N, Th-H, and U-H

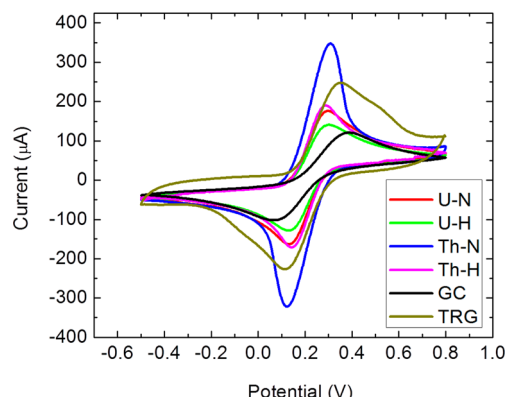


Figure 8. Cyclic voltammograms of 10 mM ferro/ferricyanide at U- and Th-doped graphene hybrids. Conditions: 50 mM PBS buffer, pH 7.0, scan rate of 100 mV/s.

TABLE 4. HET Rates Calculated Using an $[Fe(CN)_6]^{3-/-4-}$ Electrochemical Probe (Conditions Are the Same as in Figure 8)

sample	HET rate ($cm s^{-1}$)
U-N	1.78×10^{-3}
U-H	1.73×10^{-3}
Th-N	1.50×10^{-3}
Th-H	2.22×10^{-3}
TRG	6.50×10^{-4}
GC	2.04×10^{-4}

started at -0.25 V and reached its maximum at -0.36 V (Figure 9). For U-N, reduction started at -0.22 V and reached its maximum at -0.33 V. The GC and TRG controls showed weak reduction peaks; reduction started at -0.28 V and reached its maximum

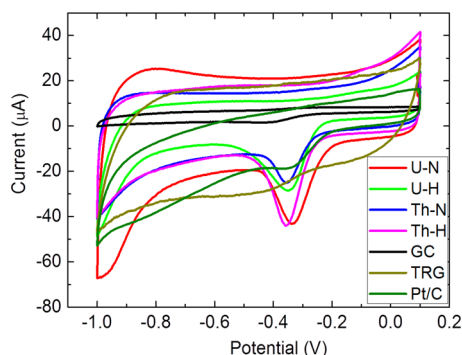


Figure 9. Electrochemical reduction of oxygen of U- and Th-doped graphene hybrids. For comparison, voltammetry at 1 wt % Pt/C is shown. Conditions: 0.1 M KOH saturated with oxygen; cyclic voltammetry scan rate of 100 mV/s.

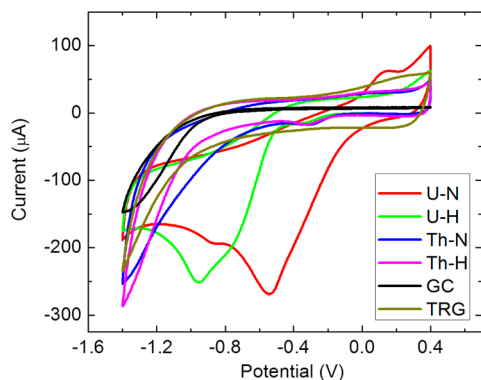


Figure 10. Electrochemical reduction of 10 mM hydrogen peroxide at U- and Th-doped graphene hybrids. Conditions: 50 mM PBS, pH 7.0; cyclic voltammetry scan rate of 100 mV/s.

at -0.44 and -0.54 V, respectively. The potential shift of 60 mV is technologically important. For comparison, we also measured ORR for a commercial 1 wt % Pt/C-modified GC electrode typically used as an industrial standard for such reactions. For this electrode, oxygen reduction started at -0.22 V and reached its peak at -0.36 V. This is very important because it shows that our U-doped graphene is practically identical, indeed even slightly superior, to the electrocatalytic properties of the commercial Pt/C catalyst at similar loading. This finding could be of huge potential industrial importance.

Electrochemical measurements were also conducted for hydrogen peroxide reduction. While a weak reduction peak (maximum at -0.32 V) was found for the Th-doped hybrids, a much more intense reduction peak was detected for the U-doped hybrids (Figure 10). For U-H, reduction started at -0.52 V and peaked at -0.85 V. For U-N, reduction started at -0.11 V and peaked at -0.54 V; a second, weaker reduction peak

was also observed at -0.85 V. No peaks were observed for the controls (GC and TRG). The high electrochemical activity of the Th- and U-doped hybrids is probably related to the formation of actinide in a mixed-valence state. This effect is most significant in the case of uranium, which suggests that uranium oxide has a crucial role to play in electron transfer in electrocatalytic reactions. Uranium and thorium compounds are broadly used in chemical catalysis.¹⁶ However, to the best of our knowledge, no previous study has compared the electrocatalytic activity of uranium and thorium. In this respect, the differences between thorium and uranium are related to their chemical behavior. Thorium's main oxidation state is Th^{4+} , but uranium is able to form compounds across a wide range of oxidation states, from U^{3+} up to U^{6+} . We suppose that its enhanced electrocatalytic activity is related to this phenomenon. It is well-known that, in the case of cerium-oxide-based electrocatalysts, the ability to change between $\text{Ce}^{3+}/\text{Ce}^{4+}$ has a significant effect on catalytic activity.³⁶

CONCLUSION

Uranium-graphene and thorium-graphene hybrids were prepared by the reaction of UO_2^{2+} and Th^{4+} ions with graphene oxide and subsequent exfoliation in hydrogen and nitrogen atmospheres. The high C/O ratios obtained from all of the analytical techniques confirmed the formation of highly reduced graphene hybrids, particularly in a hydrogen atmosphere. The hybrids contained ~ 1 wt % of actinide ions. In all samples, the actinide was uniformly distributed on the graphene sheets without the formation of agglomerates. The concentration of uranium was slightly higher than that of thorium due to the higher sorption capacity of graphene oxide toward uranyl ions. Although both of the synthesized materials exhibited significant electrocatalytic activity toward the reduction of oxygen and hydrogen peroxide, the uranium-doped hybrid possessed significantly better electrochemical properties. Furthermore, the oxygen reduction reaction electrocatalysis of the U-doped graphene was virtually identical to that of a Pt/C catalyst at the same loading. This could be of huge potential industrial importance because it represents a potential use for depleted uranium, which is currently only used in a few minor applications and is generally stored as waste. Indeed, it suggests that the use of uranium as a graphene dopant has considerable potential for application in fuel cells and other electrochemical devices.

EXPERIMENTAL SECTION

Graphene oxide was prepared from pure graphite microparticles ($2\text{--}15\ \mu\text{m}$, 99.999%, from Alfa Aesar, Germany). Sulfuric acid (98%), nitric acid (68%), potassium chloride (99%),

hydrochloric acid (37%), silver nitrate (99.5%), barium nitrate (99.5%), hydrogen peroxide (30%), and *N,N*-dimethylformamide (DMF) were obtained from Penta, Czech Republic. Potassium phosphate dibasic, potassium phosphate monobasic, potassium

ferrocyanide, and potassium chloride were obtained from Lach-Ner, Czech Republic. Active carbon with 1 wt % Pt was obtained from Sigma-Aldrich, Czech Republic. Deionized water (16.8 MΩ) was used for all syntheses. Uranyl nitrate hexahydrate and thorium nitrate pentahydrate were obtained from Lachema, Czechoslovakia. High-purity hydrogen (99.999%), argon (99.999%), and nitrogen (99.999%) were obtained from SIAD, Czech Republic.

Graphene oxide was prepared according to the Hofmann method is termed "GO".³⁷ Concentrated sulfuric acid (87.5 mL) and nitric acid (27 mL) were added to a reaction flask containing a magnetic stir bar. The mixture was then cooled at 0 °C, and graphite (5 g) was added. The mixture was vigorously stirred to avoid agglomeration and to obtain a homogeneous dispersion. While the reaction flask was kept at 0 °C, potassium chlorate (55 g) was slowly added to the mixture in order to avoid a sudden increase in temperature and the consequent formation of explosive chlorine dioxide gas. Upon the complete dissolution of the potassium chlorate, the reaction flask was then loosely capped to allow the escape of the evolved gas and the mixture was continuously vigorously stirred for 96 h at room temperature. On completion of the reaction, the mixture was poured into deionized water (3 L) and decanted. The graphene oxide was first redispersed in HCl (5%) solutions to remove sulfate ions and then repeatedly centrifuged and redispersed in deionized water until all chloride and sulfate ions were removed. The graphene oxide slurry was then dried in a vacuum oven at 50 °C for 48 h before use.

The graphene oxide (200 mg) was redispersed in water (100 mL) by ultrasonication (150 W/60 min). Thorium-doped graphene oxide was prepared by the addition of 100 mL of a solution containing 5 wt % of Th⁴⁺ (in the form of an acidified aqueous solution of thorium nitrate) to the graphene oxide dispersion. The mixture was stirred for 6 h and left to stand for the following 24 h, during which the graphene oxide absorbed the Th⁴⁺ ions from the solution. Next, it was filtered by suction and repeatedly washed with deionized water before being dried in a vacuum oven prior to further use (48 h, 60 °C). The Th-doped graphene oxide was termed "Th-GO".

Uranium-doped graphene oxide was prepared by the addition of 100 mL of a solution containing 5 wt % uranium (in the form of a slightly acidified aqueous solution of UO₂(NO₃)₂). The reaction mixture was stirred for 6 h and left to stand for the following 24 h, during which time the graphene oxide absorbed the (UO₂)²⁺ ions in the solution. Next, it was filtered by suction and repeatedly washed with deionized water before being dried in a vacuum oven prior to further use (48 h, 60 °C). The U-doped graphene oxide was termed "U-GO".

The thermal exfoliation of the doped precursors was carried out at 1000 °C for 12 min in either a nitrogen or hydrogen atmosphere. First, the precursor was placed inside a porous quartz glass capsule connected to a magnetic manipulator in a vacuum-tight quartz reactor under a controlled atmosphere. This system provided a temperature gradient of over 1000 °C min⁻¹. Then, the sample was flushed repeatedly with pure nitrogen or pure hydrogen and subsequently inserted into a preheated reactor in a nitrogen or hydrogen atmosphere (pressure: 1 atm) to produce the doped graphene hybrid. The gas flow was 1000 mL min⁻¹, which ensured the removal of reaction byproducts. Using this simple, scalable method, four samples were created and termed "U-H", "U-N", "Th-H", and "Th-N" according to dopant and exfoliation atmosphere.

The morphology was investigated using scanning electron microscopy with a FEG electron source (Tescan Lyra dual-beam microscope). Elemental composition and mapping were performed using an energy-dispersive spectroscopy (EDS) analyzer (X-Max^N) with a 20 mm² SDD detector (Oxford Instruments) and AZtecEnergy software. To conduct the measurements, the samples were placed on a carbon conductive tape. SEM and SEM-EDS measurements were carried out using a 10 kV electron beam. For the STEM measurement, the graphene was dispersed in ethanol (1 mg/mL) and 1 μL was placed on a carbon/copper 200 mesh grid.

Combustible elemental analysis was performed using a PE 2400 Series II CHNS/O analyzer (PerkinElmer, USA). The instrument

was used in CHN operating mode (the most robust and interference-free mode) to convert the sample elements to simple gases (CO₂, H₂O, and N₂). The PE 2400 analyzer automatically performed combustion, reduction, homogenization of product gases, separation, and detection. An MX5 microbalance (Mettler Toledo) was used for precise weighing of the samples (1.5–2.5 mg per single sample analysis). Using this procedure, the accuracy of CHN determination is better than 0.30% abs. Internal calibration was performed using an *N*-fenyl urea.

An inVia Raman microscope (Renishaw, England) was used for Raman spectroscopy in backscattering geometry with CCD detector. DPSS laser (532 nm, 50 mW) with 50× magnification objective was used for exciting the sample. The instrument was calibrated with a silicon reference, which gives a peak position at 520 cm⁻¹ and a resolution of less than 1 cm⁻¹.

High-resolution X-ray photoelectron spectroscopy was performed using an ESCAProbeP spectrometer (Omicron Nanotechnology Ltd., Germany) with a monochromatic aluminum X-ray radiation source (1486.7 eV). Wide-scan surveys of all elements were performed, with subsequent high-resolution scans of the C 1s, O 1s, U 4f, and Th 4f peaks. Relative sensitivity factors were used to evaluate the carbon-to-oxygen (C/O) ratios from the survey spectra. The samples were placed in a conductive carrier made from a high-purity silver bar.

All glassy carbon electrodes were cleaned by polishing with an alumina suspension to renew the electrode surface then washed and wiped dry prior to any use. The materials were dispersed in DMF as the organic solvent to obtain a 1 mg mL⁻¹ suspension. The suspension was then sonicated for 5 min at room temperature before every use. A cleaned GC electrode was then modified by coating with a 2 μL aliquot of the suspension and left to dry at ambient temperature to give a layer of randomly dispersed material on the GC surface. The modified GC electrodes, Ag/AgCl reference electrode, and platinum counter electrode were then placed into an electrochemical cell which contains the electrolyte solution, and the measurements were then taken. The electrolytes used were 50 mM, pH 7.2 phosphate buffer solution (PBS) as the blank buffer electrolyte and 10 mM ferro/ferricyanide dissolved in PBS. For the other set of experiments, we used 10 mM H₂O₂ dissolved in 50 mM PBS and oxygen-saturated 0.1 M KOH. All measurements were performed for two consecutive scans at a scan rate of 100 mV s⁻¹. The inherent electrochemistry in PBS was measured under argon atmosphere. The measurement was performed using an Interface 1000 potentiostat (Gamry, USA).

Safety Considerations. From the point of view of radiation safety, the depleted uranium and thorium used in this work are safe; their activity is less than 0.2 kBq/g of the synthesized material. However, long-term exposure to radioactive materials through ingestion (either via the oral or nasal route) can result in adverse health effects and must be avoided.

Conflict of Interest: The authors declare no competing financial interest.

Acknowledgment. This research was supported by a Specific University Research grant, MSMT No 20/2014. M.P. acknowledges a Tier 2 grant (MOE2013-T2-1-056) from the Ministry of Education, Singapore. A.M. was supported by Czech Science Foundation (Project No. P108/12/G108).

Supporting Information Available: Additional figures and table as described in the text. This material is available free of charge via the Internet at <http://pubs.acs.org>.

REFERENCES AND NOTES

- Greeley, J.; Stephens, I. E. L.; Bondarenko, A. S.; Johansson, T. P.; Hansen, H. A.; Jaramillo, T. F.; Rossmeisl, J.; Chorkendorff, I.; Nørskov, J. K. Alloys of Platinum and Early Transition Metals as Oxygen Reduction Electrocatalysts. *Nat. Chem.* **2009**, *1*, 552–556.
- Geim, A. K.; Novoselov, K. S. The Rise of Graphene. *Nat. Mater.* **2007**, *6*, 183–191.
- Wang, X.; Zhi, L.; Mullen, K. Transparent, Conductive Graphene Electrodes for Dye-Sensitized Solar Cells. *Nano Lett.* **2008**, *8*, 323–327.

4. Toh, H. S.; Ambrosi, A.; Chua, C. K.; Pumera, M. Graphene Oxides Exhibit Limited Cathodic Potential Window Due to Their Inherent Electroactivity. *J. Phys. Chem. C* **2011**, *115*, 17647–17650.
5. Pumera, M.; Ambrosi, A.; Bonanni, A.; Chng, E. L. K.; Poh, H. L. Graphene for Electrochemical Sensing and Biosensing. *Trends Anal. Chem.* **2010**, *29*, 954–965.
6. Pumera, M. Graphene-Based Nanomaterials for Energy Storage. *Energy Environ. Sci.* **2011**, *4*, 668–674.
7. Elias, D. C.; Nair, R. R.; Mohiuddin, T. M. G.; Morozov, S. V.; Blake, P.; Halsall, M. P.; Ferrari, A. C.; Boukhvalov, D. W.; Katsnelson, M. I.; Geim, A. K.; et al. Control of Graphene's Properties by Reversible Hydrogenation: Evidence for Graphane. *Science* **2009**, *323*, 610–613.
8. Jankovský, O.; Šimek, P.; Sedmidubský, D.; Matějková, S.; Janoušek, Z.; Šembera, F.; Pumera, M.; Sofer, Z. Water-Soluble Highly Fluorinated Graphite Oxide. *RSC Adv.* **2014**, *4*, 1378–1387.
9. Nair, R. R.; Ren, W.; Jalil, R.; Riaz, I.; Kravets, V. G.; Britnell, L.; Blake, P.; Schedin, F.; Mayorov, A. S.; Yuan, S.; et al. Fluorographene: A Two-Dimensional Counterpart of Teflon. *Small* **2010**, *6*, 2877–2884.
10. Giovanni, M.; Poh, H. L.; Ambrosi, A.; Zhao, G.; Sofer, Z.; Šanek, F.; Khezri, B.; Webster, R. D.; Pumera, M. Noble Metal (Pd, Ru, Rh, Pt, Au, Ag) Doped Graphene Hybrids for Electrocatalysis. *Nanoscale* **2012**, *4*, 5002–5008.
11. Liu, X.-W.; Mao, J.-J.; Liu, P.-D.; Wei, X.-W. Fabrication of Metal–Graphene Hybrid Materials by Electroless Deposition. *Carbon* **2011**, *49*, 477–483.
12. Li, Y.; Fan, X.; Qi, J.; Ji, J.; Wang, S.; Zhang, G.; Zhang, F. Palladium Nanoparticle–Graphene Hybrids as Active Catalysts for the Suzuki Reaction. *Nano Res.* **2010**, *3*, 429–437.
13. Toh, R. J.; Poh, H. L.; Sofer, Z.; Pumera, M. Transition Metal (Mn, Fe, Co, Ni)-Doped Graphene Hybrids for Electrocatalysis. *Chem.—Asian J.* **2013**, *8*, 1295–1300.
14. Lim, D.-H.; Negreira, A. S.; Wilcox, J. DFT Studies on the Interaction of Defective Graphene-Supported Fe and Al Nanoparticles. *J. Phys. Chem. C* **2011**, *115*, 8961–8970.
15. Lim, D.-H.; Wilcox, J. Mechanisms of the Oxygen Reduction Reaction on Defective Graphene-Supported Pt Nanoparticles from First-Principles. *J. Phys. Chem. C* **2012**, *116*, 3653–3660.
16. Fox, A. R.; Bart, S. C.; Meyer, K.; Cummins, C. C. Towards Uranium Catalysts. *Nature* **2008**, *455*, 341–349.
17. Kumar, D.; Bhat, R. P.; Samant, S. D.; Gupta, N. M. Uranyl-Based Heterogeneous Catalyst for the Selective Oxidation of Benzylic Alcohols To Form Corresponding Carbonyl Compounds. *Catal. Commun.* **2005**, *6*, 627–632.
18. Audi, G.; Bersillon, O.; Blachot, J.; Wapstra, A. H. The NUBASE Evaluation of Nuclear and Decay Properties. *Nucl. Phys. A* **2003**, *729*, 3–128.
19. Allen, G. C.; Holmes, N. R. Surface Characterisation of α -, β -, γ -, and δ -UO₃ Using X-ray Photoelectron Spectroscopy. *J. Chem. Soc., Dalton Trans.* **1987**, *12*, 3009–3015.
20. Allen, G. C.; Hubert, S.; Simoni, E. Optical Absorption and X-ray Photoelectron Spectroscopic Studies of Thorium Tetrabromide. *J. Chem. Soc., Faraday Trans.* **1995**, *91*, 2767–2769.
21. Ambrosi, A.; Bonanni, A.; Sofer, Z.; Cross, J. S.; Pumera, M. Electrochemistry at Chemically Modified Graphenes. *Chem.—Eur. J.* **2011**, *17*, 10763–10770.
22. Cançado, L. G.; Takai, K.; Enoki, T.; Endo, M.; Kim, Y. A.; Mizusaki, H.; Jorio, A.; Coelho, L. N.; Magalhaes-Paniago, R.; Pimenta, M. A. General Equation for the Determination of the Crystallite Size L_a of Nanographite by Raman Spectroscopy. *Appl. Phys. Lett.* **2006**, *88*, 163106.
23. Nicholson, R. S. Theory and Application of Cyclic Voltammetry for Measurement of Electrode Reaction Kinetics. *Anal. Chem.* **1965**, *37*, 1351–1355.
24. Wu, G.; Zelenay, P. Nanostructured Nonprecious Metal Catalysts for Oxygen Reduction Reaction. *Acc. Chem. Res.* **2013**, *46*, 1878–1889.
25. Jin, J.; Pan, F.; Jiang, L.; Fu, X.; Liang, A.; Wei, Z.; Zhang, J.; Sun, G. Catalyst-Free Synthesis of Crumpled Boron and Nitrogen Co-doped Graphite Layers with Tunable Bond Structure for Oxygen Reduction Reaction. *ACS Nano* **2014**, *8*, 3313–3321.
26. Jiao, Y.; Zheng, Y.; Jaroniec, M.; Qiao, S. Z. Origin of the Electrocatalytic Oxygen Reduction Activity of Graphene-Based Catalysts: A Roadmap To Achieve the Best Performance. *J. Am. Chem. Soc.* **2014**, *136*, 4394–4403.
27. Li, Q.; Noffke, B. W.; Wang, Y.; Menezes, B.; Peters, D. G.; Raghavachari, K.; Li, L.-S. Electrocatalytic Oxygen Activation by Carbanion Intermediates of Nitrogen-Doped Graphitic Carbon. *J. Am. Chem. Soc.* **2014**, *136*, 3358–3361.
28. Liang, J.; Jiao, Y.; Jaroniec, M.; Qiao, S. Z. Sulfur and Nitrogen Dual-Doped Mesoporous Graphene Electrocatalyst for Oxygen Reduction with Synergistically Enhanced Performance. *Angew. Chem., Int. Ed.* **2012**, *51*, 11496–11500.
29. Yang, S.; Feng, X.; Wang, X.; Müllen, K. Graphene-Based Carbon Nitride Nanosheets as Efficient Metal-Free Electrocatalysts for Oxygen Reduction Reactions. *Angew. Chem., Int. Ed.* **2011**, *50*, 5339–5343.
30. Liu, Z.-W.; Peng, F.; Wang, H.-J.; Yu, H.; Zheng, W.-X.; Yang, J. Phosphorus-Doped Graphite Layers with High Electrocatalytic Activity for the O₂ Reduction in an Alkaline Medium. *Angew. Chem., Int. Ed.* **2012**, *50*, 3257–3261.
31. Yang, Z.; Yao, Z.; Li, G.; Fang, G.; Nie, H.; Liu, Z.; Zhou, X.; Chen, X. A.; Huang, S. Sulfur-Doped Graphene as an Efficient Metal-Free Cathode Catalyst for Oxygen Reduction. *ACS Nano* **2012**, *6*, 205–211.
32. Li, Y.; Zhou, W.; Wang, H.; Xie, L.; Liang, Y.; Wei, F.; Idrobo, J.-C.; Pennycook, S. J.; Dai, H. An Oxygen Reduction Electrocatalyst Based on Carbon Nanotube–Graphene Complexes. *Nat. Nanotechnol.* **2012**, *7*, 394–400.
33. Sheng, Z.-H.; Gao, H.-L.; Bao, W.-J.; Wang, F.-B.; Xia, X.-H. Synthesis of Boron Doped Graphene for Oxygen Reduction Reaction in Fuel Cells. *J. Mater. Chem.* **2012**, *22*, 390–395.
34. Lin, Z.; Waller, G. H.; Liu, Y.; Liu, M.; Wong, C.-P. Simple Preparation of Nanoporous Few-Layer Nitrogen-Doped Graphene for Use as an Efficient Electrocatalyst for Oxygen Reduction and Oxygen Evolution Reactions. *Carbon* **2013**, *53*, 130–136.
35. Su, Y.; Zhang, Y.; Zhuang, X.; Li, S.; Wu, D.; Zhang, F.; Feng, X. Low-Temperature Synthesis of Nitrogen/Sulfur Co-doped Three-Dimensional Graphene Frameworks as Efficient Metal-Free Electrocatalyst for Oxygen Reduction Reaction. *Carbon* **2013**, *62*, 296–301.
36. Wei, H.; Wang, E. Nanomaterials with Enzyme-like Characteristics (Nanozymes): Next-Generation Artificial Enzymes. *Chem. Soc. Rev.* **2013**, *42*, 6060–6093.
37. Hofmann, U.; Frenzel, A. Die Reduktion von Graphitoxyd mit Schwefelwasserstoff. *Kolloid Z.* **1934**, *68*, 149–151.